NASA MEMO 10-9-58A

NASA MEMORANDUM

AN INVESTIGATION OF SOME EFFECTS OF MACH NUMBER AND AIR TEMPERATURE ON THE HYPERSONIC FLOW OVER A BLUNT BODY

By Alvin Seiff and Simon C. Sommer

Ames Research Center
Moffett Field, Calif.

[redacted]

NATIONAL AERONAUTICS AND SPACE ADMINISTRATION
WASHINGTON
February 1959

[redacted]

NATIONAL AERONAUTICS AND SPACE ADMINISTRATION

MEMORANDUM 10-9-58A

AN INVESTIGATION OF SOME EFFECTS OF MACH NUMBER AND AIR TEMPERATURE ON THE HYPERSONIC FLOW OVER A BLUNT BODY[1]

By Alvin Seiff and Simon C. Sommer

INTRODUCTION

Because of the limitations of existing test facilities, most experimental investigations of the aerodynamic problems of the ICBM have been done at Mach numbers and/or enthalpies very much below those of the missile warhead during re-entry. It has been speculated that reducing the Mach number is not injurious to simulation of the flow if the enthalpy is retained at its flight value, and further, that forces, moments, and pressures can be measured with neither Mach number nor enthalpy reproduced provided that the Mach number is high enough so that the flow field "freeze" is in effect. The basis for these arguments is partly theoretical (ref. 1) and partly a result of the common experience that pressure coefficients on forward-facing body surfaces tend to remain relatively constant above a Mach number of 4 or 5 and approach asymptotic values. For relatively blunt bodies, this "freezing" of the body pressures may occur at Mach numbers as low as 3.

While it is known that these "freeze" rules are valid in at least a limited sense, it should not be assumed prematurely that all hypersonic flows are invariant with Mach number in all important respects. For example, it has been previously pointed out that the entropy gradients in the disturbed flow field of a blunt body can be expected to vary with Mach number because of the variation in shock strength with Mach number; that is, the existence of a "shear layer" in the flow tends to become more pronounced as the Mach number is raised. Thus, a detailed examination of hypersonic flow fields should be made to determine the extent of similarity or dissimilarity to be observed as the Mach number is varied at constant enthalpy.

[1]Title, Unclassified. Originally presented at the Second Technical Symposium on Ballistic Missiles, sponsored by the Air Force Ballistic Missile Division of the ARDC, and The Ramo-Wooldridge Corporation, Los Angeles, California, June 12-14, 1957.

Important parts of the flow field about blunt objects are dependent on viscosity, and are therefore not subject to a "freeze" on the basis of any known arguments. In this category, there may be listed separated flows, including separated flow behind the body base, and boundary layers. Knowledge of the manner in which the change from supersonic to hypersonic flow conditions will affect these areas must be considered very incomplete at present.

With the object of investigating, in an exploratory fashion, the extent of similarity in both the inviscid and viscous parts of a hypersonic flow field subjected to large variations in Mach number and total enthalpy, tests were undertaken with gun-launched models in the Ames supersonic free-flight wind tunnel. The model used, shown sketched in figure 1, was chosen very blunt so as to satisfy as completely as possible the conditions necessary for observation of the flow field freeze. (Refs. 2 and 3 indicate that the body chosen also would have virtue from the standpoint of withstanding aerodynamic heating during atmospheric entry.) The threads, groove, and base pointer shown on the back of the model were incorporated to facilitate launching the model and reading angle of attack. This model was tested at Mach numbers from 3.25 to 15, with ideal-gas stagnation temperatures ranging from 1600° to 8700° Rankine. The results obtained are the subject of this report.

TESTS AND RANGE OF TEST CONDITIONS

In order to achieve the model velocities required for this investigation, a large-bore light gas gun was designed, built, and test-fired. The launch tube was of 37 mm diameter. The gun is termed a shock-heated helium gun, of the type described by Neice in reference 4, and its principle of operation is indicated in figure 2. A charge of gunpowder (up to 4 pounds maximum) is exploded at the breech end of the compression chamber, a 90 mm rifle, to create a rapidly advancing interface of powder gas which produces a strong shock wave and compresses a charge of helium in the barrel to approximately 1/15 of its initial volume. The maximum conditions attained in the helium after compression are a pressure of 40,000 psi, and a temperature (theoretically) of 15,000° R. The corresponding theoretical sound speed in the propellant gas is about 17,000 feet per second. These conditions are sufficient to accelerate a 0.1 pound mass up to 10,000 feet per second. Above this velocity, difficulty has been encountered in keeping the sabot from breaking.

By use of this gun in conjunction with the supersonic free-flight wind tunnel (in which test models are shot upstream through the wind-tunnel test section (ref. 5)), it was possible to obtain the test conditions outlined in figure 3. At a constant ideal-gas stagnation

temperature of 7300° R, the Mach number was varied from 8 to 13.7. At a constant Mach number of 8, the ideal-gas stagnation temperature was varied from 7300° to 2600° R. An auxiliary test at a Mach number of 4.4 gave the same stagnation temperature as the lower point at a Mach number of 8. To represent the condition of a relatively cold, low Mach number experiment, the test condition at a Mach number of 3.25 with a stagnation temperature of 1600° R was selected. To determine the effect of the highest Mach number, highest stagnation temperature that could be attained, the maximum performance point (with present equipment) at a Mach number of 15 and a stagnation temperature of 8700° R was included.

This range of test conditions was obtained by properly varying the launching velocity of the models while choosing from the available air-flow conditions of the wind tunnel (which may be operated with no flow or with supersonic air flows at Mach numbers of 2 or 3). The static air temperature in the test section is in this way varied from 530° to 189° R, and this variation was instrumental in permitting the large changes in stagnation temperature at a given Mach number and changes in Mach number at a given stagnation temperature.

The "real-gas" conditions in the disturbed flow field were computed for the assumed condition of thermodynamic and chemical equilibrium immediately behind the shock wave. The enthalpy levels were sufficiently high to cause partial dissociation of oxygen but not of nitrogen, and also to cause reaction of nitrogen and oxygen to form nitric oxide. This reaction is favored by high pressures, and the stagnation pressures in the present experiments ranged up to 84 atmospheres, so that considerable NO formation would occur at equilibrium. The chemical state of the gas at the stagnation point was estimated with the aid of tables prepared by McKowen of Bell Aircraft Corporation (ref. 6), and is shown in figure 4. For the constant enthalpy series, roughly 15 percent of the oxygen atoms are combined in NO at equilibrium as shown by the filled circles, and another 4 to 5 percent are nascent or uncombined oxygen atoms as shown by the open circles. There was some small variation in these percentages which could be attributed to variations in the stagnation pressure from 32 to 84 atmospheres. In the series at $M_\infty = 8$ with enthalpy varying (triangular symbols) the computed NO content varied from essentially zero at the lowest enthalpy to 15.4 percent at the highest (filled triangles), while the dissociated oxygen was similarly varying from 0 to 4.1 percent (open triangles). The increase in enthalpy in going from the constant enthalpy series to the Mach number 15 test condition had an appreciable further effect. It caused the oxygen bound in NO to increase to 19 percent, and the dissociated oxygen to rise to about 11 percent. Simultaneously, significant variations in c_p and γ take place. If c_p is computed with only the pressure fixed, composition variable, it takes on values as high as 1.75 times its normal room temperature value. This is partly due to vibrational heat capacity, and

the remainder to the heat of the dissociation and nitric oxide reactions. Correspondingly, γ becomes appreciably less than 1.4, and takes on a minimum value just under 1.2 as shown in the lower part of the figure.

The absorption of heat into molecular vibration and dissociation reduces the stagnation temperatures below their ideal-gas values to the extent shown in figure 5, where the stagnation temperatures for the gas in chemical and thermodynamic equilibrium are plotted and compared with those shown previously for the ideal gas. As would be expected, the difference is greatest at the highest temperatures. At a Mach number of 15, the stagnation temperature decreases from 8700° R for an ideal gas to about 6600° R at chemical and thermodynamic equilibrium.

Under these conditions, then, test flights were made of the subject model, and the flow fields were photographed using shadowgraph optics. Accurate time measurements of the shadowgraph spark intervals from nine stations, each viewing the side and top views of the model, together with position and attitude measurements from the pictures gave information on the drag and pitching moment.

RESULTS AND DISCUSSION

A representative shadowgraph picture, obtained with a standard parallel-light shadowgraph optical system, is shown in figure 6 for a resultant Mach number of 10.0 in the Mach number 2 air stream. A background of wind-tunnel-wall turbulence is evident on the windows, and oversensitivity of the shadowgraph system causes the shock wave to appear so broad that it overlaps the model face. Aside from the bow-shock-wave outline, other things that can be seen include the boundary layer coming off the model base, the wake outline, the trailing shock waves, and the first Mach line in the Prandtl-Meyer fan at the corner of the base. To improve the view of the model so as to allow observation of the boundary layer on the front face and measurement of the shock-wave standoff distance, a focused shadowgraph arrangement was employed on four stations. The object of this arrangement is to reduce the shadowgraph sensitivity by effectively locating the photographic plate only an inch or two from the plane of flight, that is, well inside the wind tunnel. This is accomplished by use of a 6-inch-diameter mirror, serving the same function as a lens, to bring the photographic plate in focus on the desired plane inside the wind tunnel. The result obtained for focus about 3 inches from the plane of flight is shown in figure 7, which is a picture of the same model shown in figure 6, and was obtained at the adjacent station where the Mach number was 10.1. The shock image thickness is now considerably reduced and the model outline is reproduced essentially undistorted. Note the faithful reproduction of such details as the base pointer, groove, and threads. Other parts of the flow field such as the

wake and trailing shock wave have, however, become only faintly visible, so that combined use of the two types of pictures yields the maximum over-all information.

A comparison of focused pictures for two widely different Mach number and total temperature conditions is given in figures 8 and 9. Figure 8 shows the flow field for a Mach number of 6.8 with the Mach number 3 air stream, and figure 9, a Mach number of 15.1 in the same air stream. The most apparent change is a reduction in the shock-wave standoff distance by an appreciable amount. The part of the wave in front of the body appears also to be somewhat flatter at the higher Mach number but this is to a large extent an illusion as will be shown later. Detailed measurements of the wave coordinates and standoff distances were made and will be given subsequently.

The measured drag coefficients are given in figure 10. The total drag is remarkably constant for the full range of test conditions. All measurements fall between 1.01 and 1.07, a total variation of 6 percent. The drag is 10 to 15 percent less than that given by Newtonian theory modified by use of the pitot-pressure coefficient in place of the constant coefficient 2, again indicating, as in reference 10, that this theory is adequate for first approximation.

For present purposes, it was desired to isolate the pressure drag of the front face and to examine it as closely as the accuracy of measurement would permit for effects of Mach number and total enthalpy. Therefore, the base drag was estimated according to an assumption, which will be discussed in a later paragraph, (see lower curve, fig. 10) and subtracted from the total drag, and the resulting points were plotted at the enlarged scale shown in figure 11. It can be readily shown that the skin friction contributes negligibly to the total drag so that the data given in this figure are representative of the pressure drag. Now, largely because of the decrease of base-drag coefficient with increasing Mach number, but also because of a tendency of the total drag to begin to increase at the highest Mach numbers, we find a systematic increase in the pressure drag with increasing Mach number. The rate of increase exceeds the rate of increase of pitot pressure with rising Mach number, as indicated by the curve proportional to pitot pressure which is made to pass through the data at a Mach number of 15. In figure 11, increasing Mach number is generally accompanied by increasing stagnation enthalpy, as may be seen from the numbers alongside the data points, which give the stagnation enthalpies for the individual points in Btu/lb. It is therefore difficult to judge, from this figure, whether the increase in pressure drag is caused by the increase in free-stream Mach number or the corresponding increase in total enthalpy. It can be noted, however, that in the series at a nominal Mach number of 8 and also in the group of four points near a Mach number of 14, high drag tends to be associated with high enthalpy (and within each of these groups of points, the base-drag correction was nearly constant). Also, the points of highest enthalpy

at a nominal Mach number of 8 have about the same pressure drag as points of comparable enthalpy at a Mach number of 10.5. These observations suggest that the data might better be correlated on a plot with total enthalpy as independent variable, and such a presentation of the data is made in figure 12. In this figure, within the group of points at a total enthalpy below 1000 with Mach numbers from 4.3 to 8.0, it can be seen that there is no systematic effect on the drag coefficient of Mach number or total enthalpy. These points are for air which is vibrating but not dissociating or chemically reacting. Above a total enthalpy of 1400 Btu/lb, nitric oxide formation and oxygen dissociation begin to be important, and a definite increment in pressure drag is observed. Note that there are points for Mach numbers between 7 and 8 on both sides of this boundary, and that each correlates with its own group within the scatter. Within the group at total enthalpies from 1400 to 1800 and Mach numbers from 7 to 11, there is no systematic effect of Mach number. The points for Mach numbers higher than 11 also have significantly higher total enthalpies. From all these indications, it appears that the total enthalpy is playing a more significant role in fixing the pressure drag than is the Mach number.

There is one data point that does not correlate with the other data in figure 12, and that is the point for a Mach number of 3.3. Although the base-drag correction is, at this Mach number, relatively large and therefore capable of causing an error in the estimate of pressure drag, the point is believed to lie far enough off the correlation curve to indicate an effect of Mach number. It is at about this Mach number that the curve of pitot pressure begins to fall off rapidly. It appears then for the present model that the test Mach number should be greater than 4 for accurate simulation of the drag at hypersonic velocities, and that for cases where gas dissociation and chemical reaction will be involved, the total enthalpy should be simulated as well.

Now it is known from the theory of normal shock waves in a real gas that the static pressure behind the shock wave is greater for the real gas than for an ideal gas with $\gamma = 1.4$. This is, of course, consistent with the observed result that the drag is somewhat higher for the real gas. The calculated ratios of pressure behind a normal shock wave for the real gas to the pressure for the ideal gas are shown in figure 13 plotted as a function of γ downstream of the shock wave and, in the lower part of the figure, as a function of the total enthalpy. The pressures rise, for the real-gas conditions of this test, to a maximum about 5 percent higher than for the ideal gas. The shape of this curve is, however, somewhat different from that of the pressure drag curve, as can be seen by comparing the lower part of figure 13 with figure 12. By applying the pressure ratios of figure 13 as an approximate correction to the data of figure 12, we can attempt to correct the data to ideal gas conditions. The result of doing this is shown in figure 14. The correction, while it reduces the range of variation of the data, is not large enough to make a level drag curve, independent of total enthalpy.

This indicates that changes in the flow field, in addition to the changes in the vicinity of the stagnation point where the normal shock correction is most applicable, are occurring, and it is believed that the remaining increase in drag is attributable to an increase in pressures on the body sides with increasing total enthalpy.

It is pertinent to discuss the effect of the assumed variation of base drag with Mach number on these results. The values of base drag plotted in figure 10 and used in figures 11 and 12 were based on the classical premise that the base pressure tends toward zero as the Mach number becomes infinite. Values of base pressure selected ranged from 20 percent of free-stream static pressure at a Mach number of 4 to 10 percent at a Mach number of 15. Now it has been pointed out (ref. 7) that the base pressure behind blunt bodies does not continually decrease with increasing Mach number, but at very high Mach numbers, starts to increase to values in excess of stream static pressure. Base pressure higher than stream pressure, according to usual convention, will be regarded as producing thrust rather than drag, and the base-drag coefficient will be considered negative. Therefore, for this condition, the pressure drag given by $C_D - C_{D_b}$ will become larger than the values plotted in figures 11 and 12. Since this anomalous base pressure is expected to occur only at the highest test Mach numbers, its effect will be to accentuate the observed variation in pressure drag. If, for example, it is assumed that at $M = 15$, the base pressure is 10 times stream static pressure, the value of wave drag calculated from the experiment becomes increased to 1.14 (compare with fig. 12). Thus, lack of precise information on the base pressure can affect the degree of variation of the pressure drag but not the general trend of variation.

The measurements of pitching moment (as calculated from the pitching frequency) are shown in figure 15. The pitching moment is constant within the scatter of the data over the entire range of conditions of this test. It will be noted, however, that the scatter is appreciably greater than in the case of the drag measurements. The Newtonian estimate is, in this case, about as much below the data as it was above the data in the case of the drag coefficient. However, we have observed in earlier investigations that the Newtonian theory gives an initial pitching-moment curve slope of zero for the case of a right circular cylinder flown with a flat face forward, while experimentally, the right circular cylinder develops appreciable stability at zero angle of attack. This is due to the fact that pressure variations occur across the flat face at angle of attack and are stabilizing; that is, the axial force is eccentric on the front face and contributes to the stability. This has been confirmed by pressure-distribution tests in the Ames 6-inch heat-transfer wind tunnel. In contrast to this, the pitching moment computed here is attributed theoretically almost entirely to the corner and sides of the model and the contribution of the front face is computed to be zero. If we add to this computed result the experimentally determined C_{m_α} of the right

circular cylinder, with allowance for the fact that the flat portion of the present model has a diameter equal to about 0.6 of the total diameter, we obtain the upper curve, which now overestimates the measured stability somewhat. With respect to the pitching-moment data, we cannot make any further close examination such as was possible in the case of the drag because the accuracy of the data will not permit it.

Measurements were made to determine the effect of Mach number and stagnation enthalpy on the shock-wave standoff distance. From theory (see, e.g., refs. 8 and 9), it is known that the standoff distance for a given body shape is a function primarily of the air density ratio across the shock wave, which is in turn a function of the Mach number and the ratio of specific heats. For an ideal gas with constant γ, the density ratio across a normal shock wave approaches the limiting value $(\gamma+1)/(\gamma-1)$ as the Mach number becomes infinite, giving a limiting density ratio of 6 for air considered as an ideal gas. For the real gas, the density ratio can exceed 6 (up to 7.8 in the present tests if the air attains equilibrium behind the wave), and the shock wave can approach closer to the body.

The measurements were made from the focused shadowgraphs for the most part. To evaluate the distortion in location of the model face due to refraction, comparison was made in two cases of measurements from focused and unfocused shadowgraph pictures and it was found that they agreed within 1 percent of the standoff distance. The errors of measurement are believed, therefore, to be small. The data obtained are plotted in figure 16(a) as a function of the density ratios computed for chemical and thermodynamic equilibrium, and correlate in a very smooth curve. The standoff distance diminishes from 0.19d to 0.13d within the range of test conditions. Comparison is made with the theoretical results of Probstein and Lighthill (refs. 8 and 9) for standoff distances with right-circular cylinders (flat face forward) and spheres, respectively. These configurations bracket the geometry of the present model, so that the theoretical curves are at least qualitatively consistent with the measurements.

If the density ratios are calculated assuming the flow frozen with $\gamma = 1.4$, figure 16(b) is obtained. In this case, the scatter of the data is somewhat greater, comparatively large changes in standoff distance are observed to correspond to small changes in density ratio, and the agreement in trend with the theories is not as satisfactory. These factors are believed to indicate that the former assumption, chemical and thermodynamic equilibrium in the disturbed flow field, is the more accurate one.

The shapes of the shock waves, measured from the shadowgraphs with a reading accuracy of 0.0004 diameters, are reproduced in figure 17. The main source of inaccuracy in the data was not error of measurement, but angle of attack of the model. Pictures were selected for measurement

on the basis of small angle of attack and clarity and definition. The angles of attack in the plane of the photograph were always less than 1°, but in the other plane ranged from 1.0° at $M = 3.48$ to 4.5° at $M = 15.14$. The x axis was taken to be the model axis of symmetry and measurements were made on both sides of the model, both above and below the axis. The readings from the two sides can be readily identified in the Mach number 7.7 and 15.1 data, and a fairing between the two sets was made to approximate the wave shape for $\alpha = 0$.

Since the standoff distances varied, the waves have been translated to coincide at their forwardmost points to allow more detailed comparison of shape. The waves coincide out to $y = 0.4d$ and then begin to diverge. However, the difference in wave shape between Mach numbers of 7.7 and 15.1 is everywhere small. For these two rounds, the total velocity of the model through the air differed by only about 15 percent, being 8,720 ft/sec and 10,260 ft/sec, respectively. It would appear to be indicated that the sound speed in the free stream has very little influence on the wave shape provided that the total velocity of the model through the air is unchanged.

It is interesting that the shock wave is of nearly constant shape in the inner region, but that its distance from the body changes markedly as the Mach number and enthalpy are varied. The changes in density ratio across the shock wave likewise require changes in disturbed flow velocity and flow direction. Where the shock wave is normal, the velocity ratio is, to satisfy continuity, the inverse of the density ratio. Where the shock wave is oblique, the same is true of the normal component of velocity. Since the normal component downstream of the oblique wave depends on the Mach number and enthalpy but the parallel component does not, changes in downstream flow direction must result. The whole disturbed flow field, except for the shock wave, is therefore stretched or compressed according to the particular values of Mach number and enthalpy. The velocities and velocity gradients are altered.

To explore the variations that occurred in the viscous parts of the flow field, the shadowgraph pictures were examined for changes in the geometry of the wake and for the location of the boundary-layer transition point. The observed dependence of the wake convergence angle on Mach number, enthalpy, and Reynolds number is indicated in figure 18. The circular symbols represent tests at constant total enthalpy and constant Reynolds number and indicate an effect of Mach number on the wake angle. The wake becomes more convergent as the Mach number is increased. (The boundary layer coming off the base was turbulent in these cases.) At a Mach number of 8 there is an indication of the separate effects of total enthalpy and Reynolds number. Changing the total enthalpy by a factor of 2 (circles and triangles) at constant Reynolds number had very little effect on the wake geometry, whereas a further reduction in enthalpy by 1/3 together with a reduction in Reynolds number from 5 million to 3 million produced a measurable increase in convergence angle (square

symbols). This suggests the continuing importance of the Reynolds number at these flight speeds. Finally, comparison of the square symbols at Mach numbers of 4 and 8 indicates again a substantial effect of Mach number when total enthalpy and Reynolds number are held fixed. This large change was probably due to an observed increase in the extent of laminar flow at the higher Mach number. Thus, it is evident that the wake geometry depends on Mach number, Reynolds number, and transition location, but in the range covered here, is essentially independent of total enthalpy.

Evidence of the location of boundary-layer transition to turbulence was sought by use of the methods outlined in reference 10. Although the model surfaces were not individually inspected and carefully controlled, a relatively high polish was applied with emery polishing papers (type I surface of reference 10). The majority of the tests were conducted at a Reynolds number of 5 million based on free-stream properties and diameter, and in these tests, transition occurred in the region of the rounded corner or on the sides of the front face. In the test at a Mach number of 8, with the lowest stagnation temperature, 2400° Rankine, the Reynolds number was 3 million instead of 5 million, because of the pressure limitation of the facility, and a fully laminar flow to a point well behind the model base was observed. It should be noted, however, that when these same conditions were obtained at a free-stream Mach number of 4.25 instead of 8, fully laminar flow was not obtained - transition occurred on the sides of the front face. To fully evaluate the causes of these changes - that is, to separate the effects of free-stream Mach number, Reynolds number, stagnation temperature, and surface roughness - was beyond the scope of the present investigation.

Of particular interest in the present tests was the effect of dissociation and the NO reaction on boundary-layer transition. Examination of the pictures at high enthalpy failed to indicate any significant effect of extending the tests into this region. Transition tended to occur at the shoulder or on the sides of the front face for cases with or without dissociation as long as the Reynolds number was held at 5 million. This is a relatively high Reynolds number for models of this scale, and roughness could be the controlling factor causing transition. In any case, it can be concluded that for the conditions of this test, the occurrence of a moderate degree of dissociation and chemical reaction did not influence the location of boundary-layer transition.

CONCLUDING REMARKS

Some exploratory experiments to define effects of Mach number and enthalpy on the flow field about a blunt body, at Mach numbers ranging from moderately supersonic to well into the hypersonic speed range have been described. At the highest enthalpy attained, 30 percent of the

oxygen will have dissociated or entered into nitric oxide at chemical equilibrium. While certain of the parameters were observed to be relatively constant over the range covered, others underwent measurable changes. The pressure drag, while relatively constant, showed a systematic dependence on the total enthalpy and had the most rapid variation at the highest enthalpies of the test. On the other hand, it showed very little dependence on the Mach number, with enthalpy fixed, as long as the free-stream Mach number was greater than 4.3. The gross view of the pitching-moment data showed about the same constancy as the total drag, and the accuracy of the pitching-moment data did not permit really close examination for small variations. Measurement of the shock-wave shapes and standoff distances showed that the waves were of remarkably constant shape in the inner region (extending out approximately to the body edge), but diverged farther out. The standoff distances underwent a variation by a factor of 1-1/2 within the range of the test conditions, and could be correlated as a function of the density ratio across the normal shock wave, computed assuming chemical and thermodynamic equilibrium. This interesting result, a shock wave of nearly fixed geometry moving relative to the body, leads to the requirement that the flow velocities and flow directions adjust to fit the downstream density and shock-location conditions.

In contrast to the drag, the separated flow behind the body base appeared to depend very little on the enthalpy, but did depend on the Mach number, Reynolds number, and transition point. It was found that increasing the Mach number always caused the wake to converge more rapidly. Boundary-layer transition location did not show any detectable response to the oxygen dissociation and NO formation occurring in these tests. However, additional experiments will be required to investigate this question in detail.

NOTATION

C_D total-drag coefficient

C_{D_b} base-drag coefficient

C_{m_α} pitching-moment curve slope, per radian (based on maximum model diameter)

c_p specific heat at constant pressure, Btu/lb $^\circ$R

C_{p_t} pitot-pressure coefficient

d model base diameter, ft

H total enthalpy, Btu/lb

[redacted]

l model forebody length, ft

M_a Mach number of wind-tunnel air stream

M_∞ free-stream Mach number

r model base radius, ft

R Reynolds number (based on maximum model diameter)

T temperature, $^\circ R$

T_∞ free-stream static temperature, $^\circ R$

x axial distance, ft

y radial distance, ft

γ ratio of specific heats

Δ shock-wave standoff distance, ft

ρ_1 air density downstream of normal shock wave, slugs/cu ft

ρ_∞ free-stream air density, slugs/cu ft

θ_w wake convergence angle, initial included angle between the two sides of the wake, deg

Subscripts

i ideal gas

r real gas

s stagnation point

Ames Research Center
National Aeronautics and Space Administration
Moffett Field, Calif., June 13, 1957

[redacted]

REFERENCES

1. Oswatitsch, Klaus: Similarity Laws for Hypersonic Flow. KTH Aero TN 16, Royal Inst. of Tech., Div. of Aeronautics, Stockholm, Sweden, 1950.

2. Canning, Thomas N., and Sommer, Simon C.: Investigation of Boundary-Layer Transition on Flat-Faced Bodies of Revolution at High Supersonic Speeds. NACA RM A57C25, 1957.

3. Carter, Howard S., and Bressette, Walter E.: Heat-Transfer and Pressure Distribution on Six Blunt Noses at a Mach Number of 2. NACA RM L57C18, 1957.

4. Neice, Stanford E., and Carson, James A.: Simulation of the Atmospheric Entry of Ballistic Missiles. BRL Rep. No. 1005, pt. II, Aberdeen Proving Ground, Md., Mar. 1957.

5. Seiff, Alvin: A Free-Flight Wind Tunnel for Aerodynamic Testing at Hypersonic Speeds. NACA Rep. 1222, 1955.

6. McKowen, Paul: The Equilibrium Composition and Flow Variables for Air Dissociated by a Strong Shock Wave. Bell Rep. No. 02-984-040, Bell Aircraft Corp., Mar. 1957.

7. Ferri, A., and Pallone, A.: Note on the Flow Fields on the Rear Part of Blunt Bodies in Hypersonic Flow. WADC TN 56-294, July 1956.

8. Probstein, Ronald F.: Inviscid Flow in the Stagnation Point Region of Very Blunt-Nosed Bodies at Hypersonic Flight Speeds. WADC TN 56-395, Brown Univ., Div. of Eng., 1956.

9. Lighthill, M. J.: Dynamics of a Dissociating Gas. Part I - Equilibrium Flow. Jour. Fluid Mech., vol. 2, pt. I, Jan. 1957.

10. Seiff, Alvin, Sommer, Simon C., and Canning, Thomas N.: Some Experiments at High Supersonic Speeds on the Aerodynamic and Boundary-Layer Transition Characteristics of High-Drag Bodies of Revolution. NACA RM A56I05, 1957.

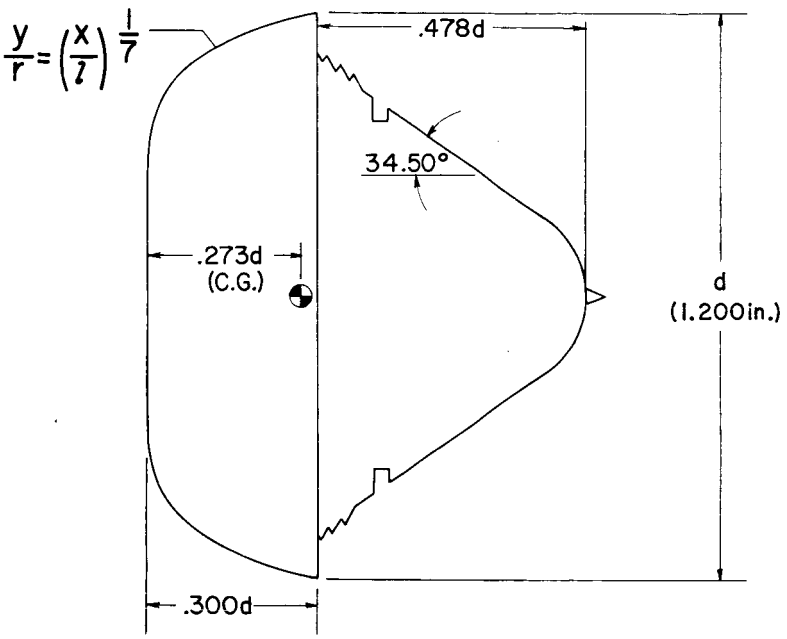

Figure 1.- Test model.

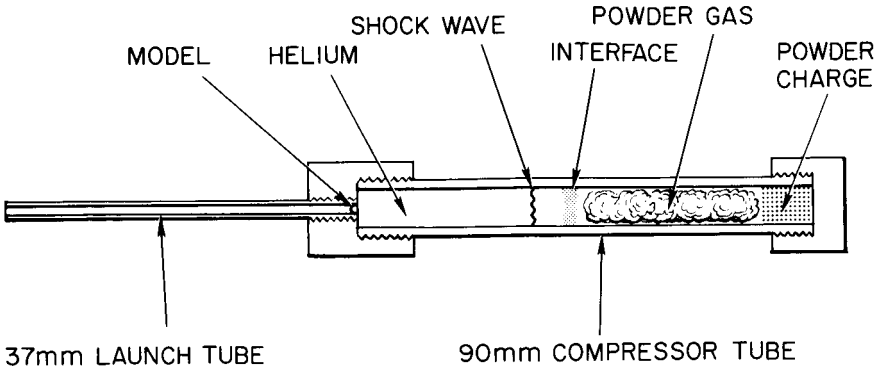

Figure 2.- Schematic diagram of 37-mm shock-heated helium gun.

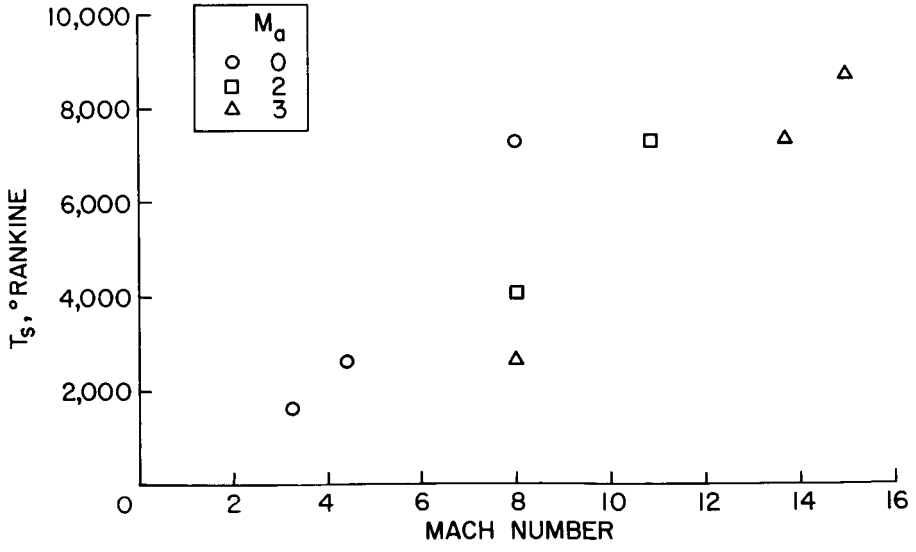

Figure 3.- Test Mach number and stagnation temperatures assuming γ and c_p constant.

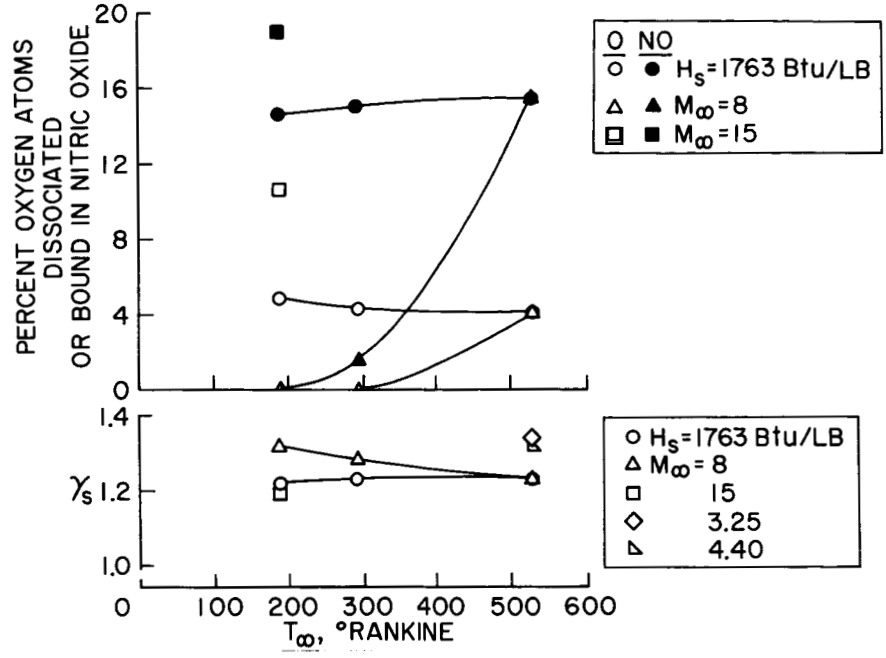

Figure 4.- Chemical and thermodynamic properties of the gas at the stagnation point assuming equilibrium.

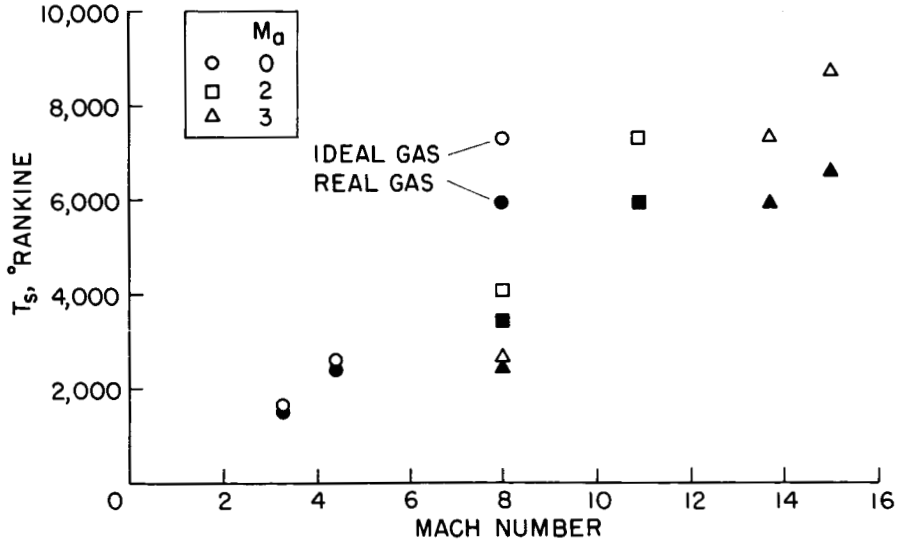

Figure 5.- Stagnation temperatures assuming chemical and thermodynamic equilibrium behind normal shock wave.

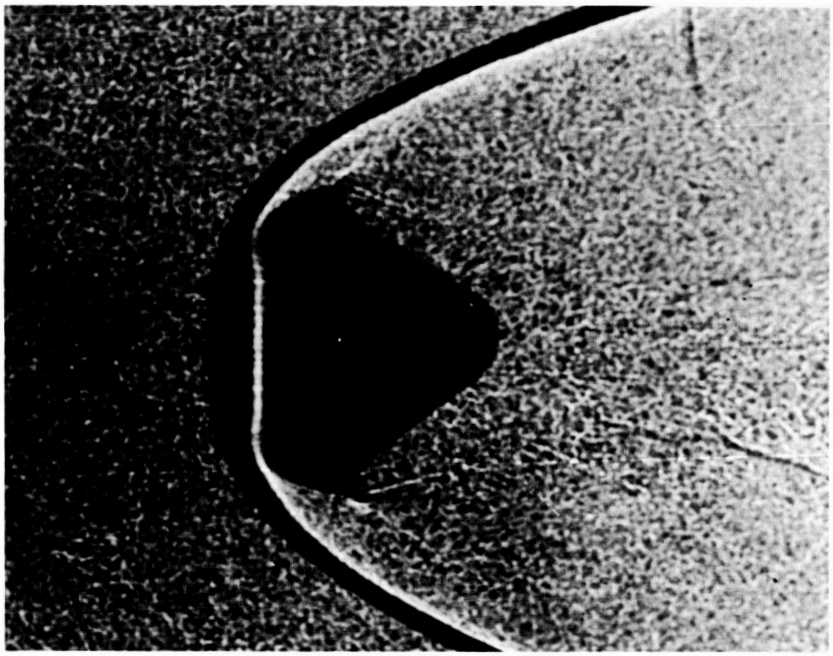

Figure 6.- Standard shadowgraph, M_∞ = 10.0.

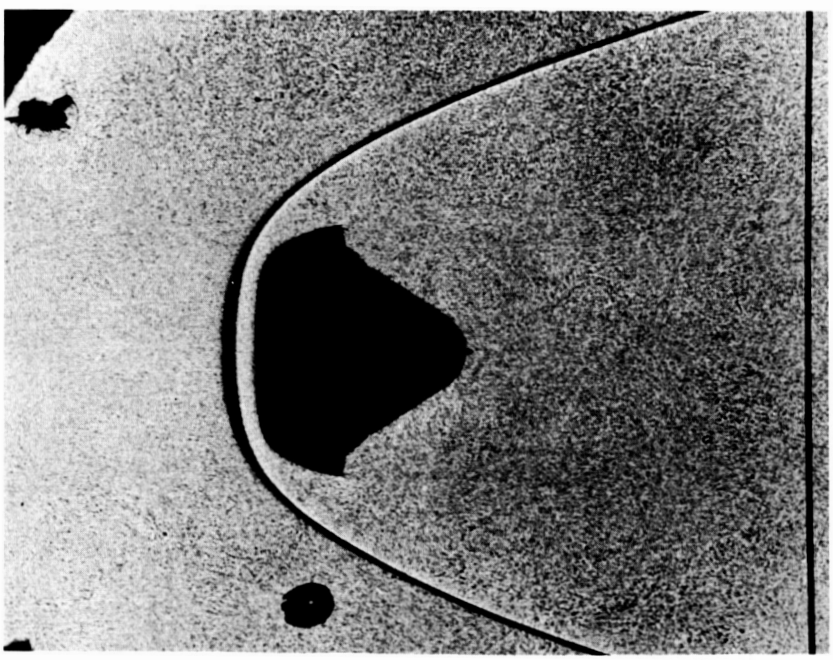

Figure 7.- Focused shadowgraph, M_∞ = 10.1.

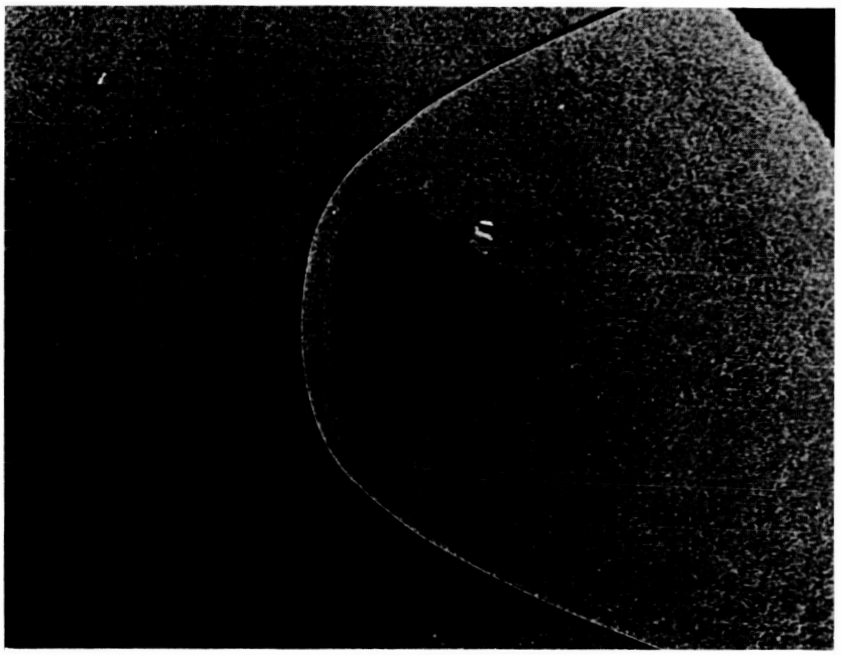

Figure 8.- Focused shadowgraph, $M_\infty = 6.8$.

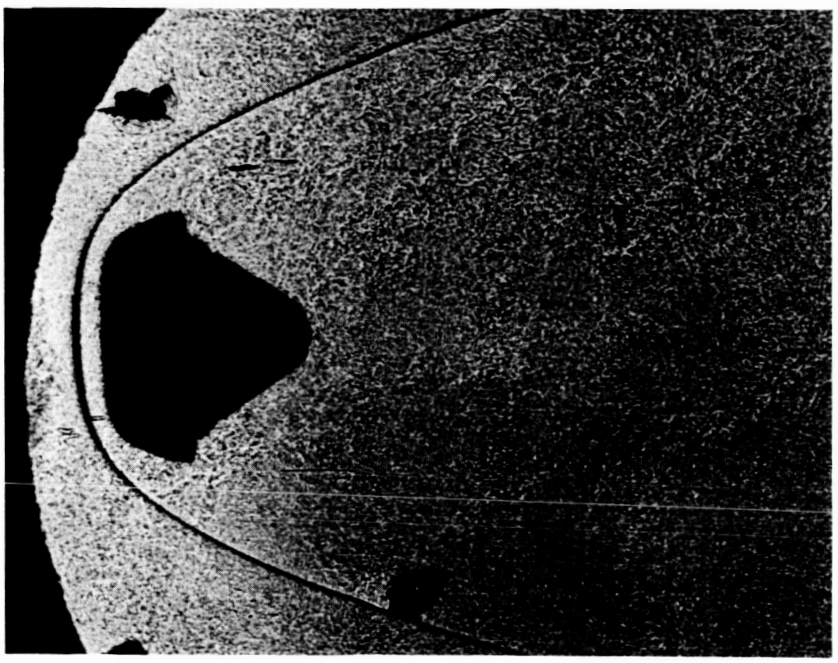

Figure 9.- Focused shadowgraph, $M_\infty = 15.1$.

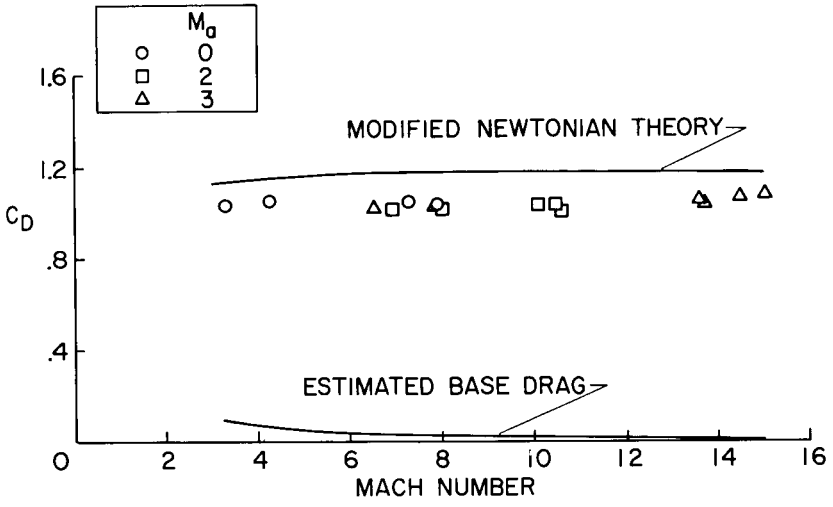

Figure 10.- Drag data.

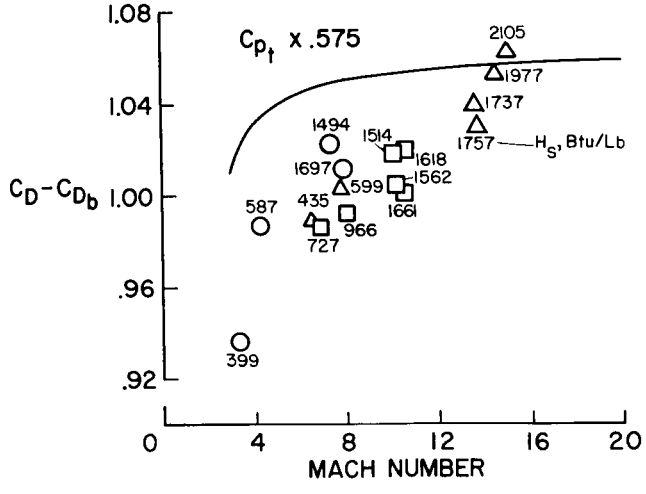

Figure 11.- Total drag minus estimated base drag.

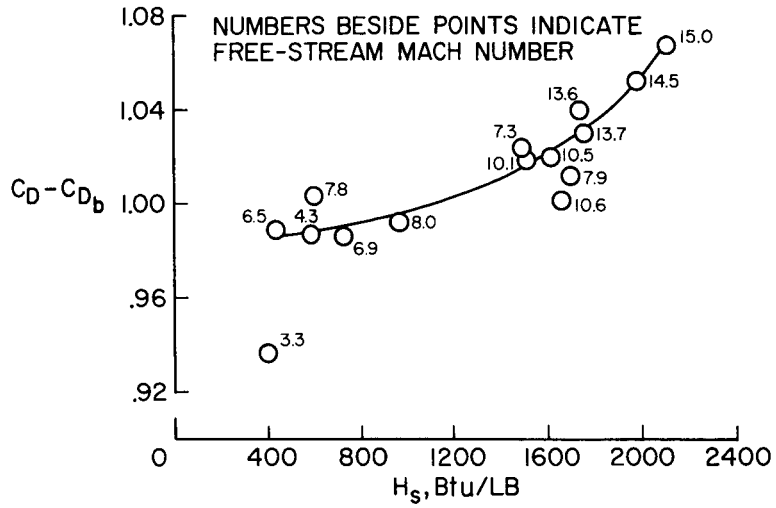

Figure 12.- Correlation of pressure drag with stagnation point enthalpy.

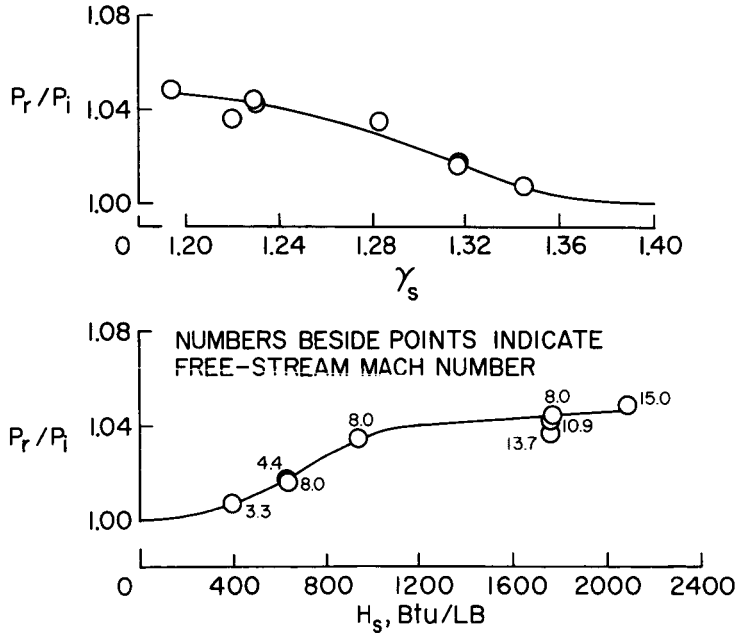

Figure 13.- Dependence of pressure downstream of normal shock wave on total enthalpy and γ.

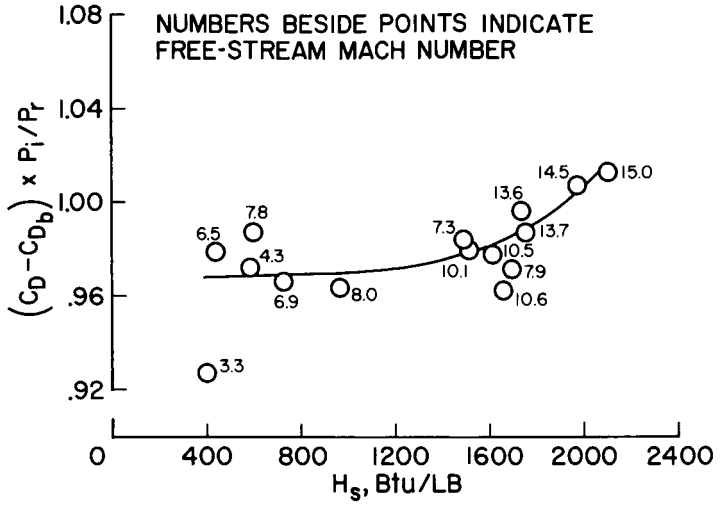

Figure 14.- Data of figure 12 corrected by pressure ratios of figure 13.

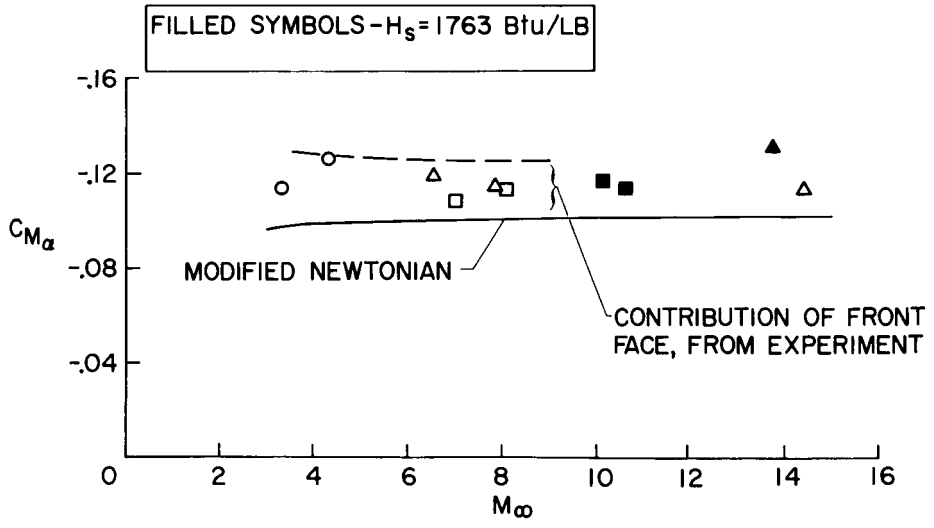

Figure 15.- Pitching-moment data.

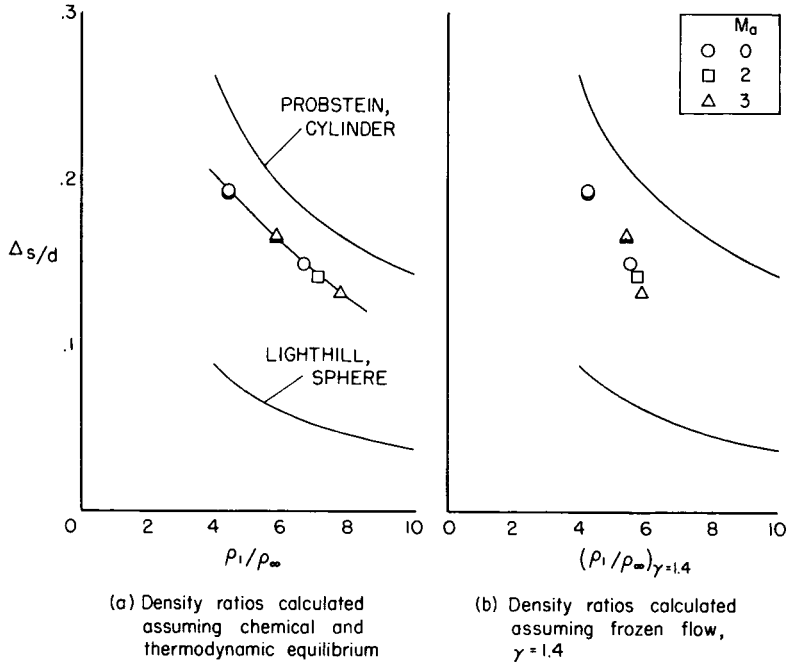

(a) Density ratios calculated assuming chemical and thermodynamic equilibrium

(b) Density ratios calculated assuming frozen flow, $\gamma = 1.4$

Figure 16.- Shock-wave standoff distance at the stagnation point.

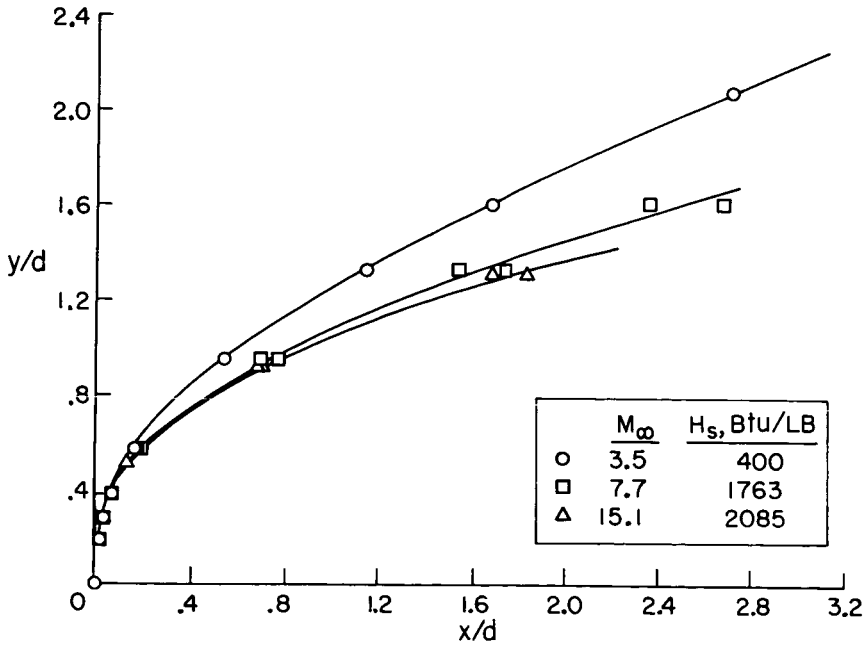

Figure 17.- Shock-wave coordinates.

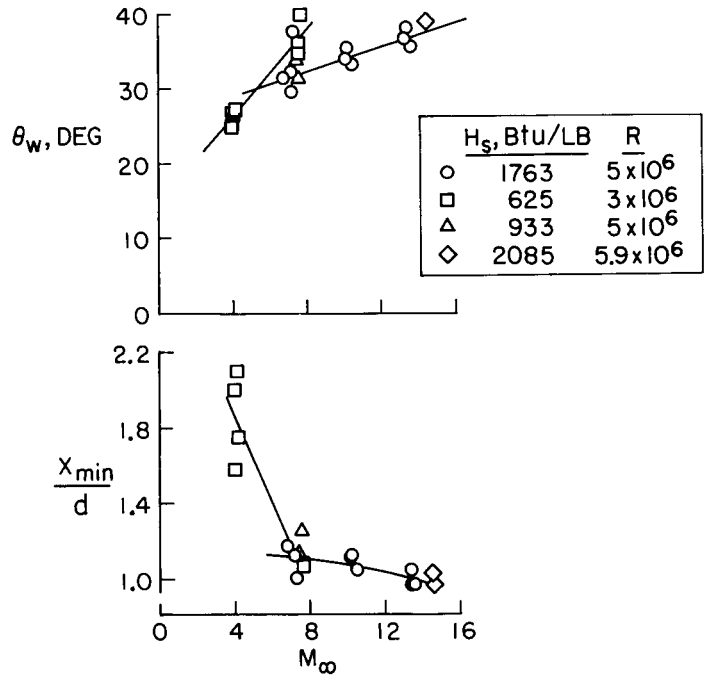

Figure 18.- Wake-convergence angle data.